

Free Energy Landscape of Protein-like Chains with Discontinuous Potentials

Hanif Bayat Movahed^{a,*}, Ramses van Zon^{a,b,†} and Jeremy Schofield^{a,‡}

^a*Chemical Physics Theory Group, Department of Chemistry,
University of Toronto, 80 St. George Street, Toronto, Ontario M5S 3H6, Canada*

^b*SciNet High Performance Computing Consortium, University of Toronto,
256 McCaul Street, Toronto, Ontario M5T 1W5, Canada*

(Dated: March 26, 2012)

In this article the configurational space of two simple protein models consisting of polymers composed of a periodic sequence of four different kinds of monomers is studied as a function of temperature. In the protein models, hydrogen bond interactions, electrostatic repulsion, and covalent bond vibrations are modeled by discontinuous step, shoulder and square-well potentials, respectively. The protein-like chains exhibit a secondary alpha helix structure in their folded states at low temperatures, and allow a natural definition of a configuration by considering which beads are bonded. Free energies and entropies of configurations are computed using the parallel tempering method in combination with hybrid Monte Carlo sampling of the canonical ensemble of the discontinuous potential system. The probability of observing the most common configuration is used to analyze the nature of the free energy landscape, and it is found that the model with the least number of possible bonds exhibits a funnel-like free energy landscape at low enough temperature for chains with fewer than 30 beads. For longer proteins, the landscape consists of several minima, where the configuration with the lowest free energy changes significantly by lowering the temperature and the probability of observing the most common configuration never approaches one due to the degeneracy of the lowest accessible potential energy.

I. INTRODUCTION

Statistical mechanical modeling has helped significantly in addressing the question of why protein folding occurs so rapidly in spite of the astronomically large number of possible configurations available to a protein. It has been suggested that folding occurs on funnel-shaped energy landscapes rather than involving a single microscopic pathway through a complicated landscape¹. Onuchic, Dill, Wolynes and co-workers proposed that a “folding funnel” is the special characteristic of foldable proteins that directs the folding protein into the native state without the need for a definite pathway^{2–9}. According to this picture, topological features of the free energy landscape, defined in a coarse-grained sense by averaging over conformations of the protein with similar characteristics, assist the folding process by channeling or funneling the evolution of configurations. The folding of a protein is viewed as a process in which the protein glides down in the funnel-shaped free-energy landscape as the temperature drops or as time progresses along a multitude of different paths towards its native structure^{6,7,9,10}. According to this viewpoint, structures with low free energies are situated within a basin of a broad energy valley and a protein in a configuration associated with one of the valleys can move quickly in the funnel to the lowest free energy state.

Of course the true free energy landscape is never a simple funnel, and the configurational space of a protein is a highly multi-dimensional space. Even for small proteins, its dimensionality ranks in the several hundreds¹¹. Within this high dimensional space, the free energy landscape can feature many local minima separated by energetic and entropic barriers.

Although the free energy landscape of proteins is often considered to be a key component in understanding the mechanisms of protein folding, the characterization of the structure of the free energy landscape is nebulous due to the difficulty of identifying the relationship between different conformations of proteins and determining whether particular configurations are within the same configurational basin. The difficulty of identifying conformations of proteins is compounded by the computational challenge of achieving converged sampling of available configurations for realistic protein models.

In this paper, studies of the energy landscape of a protein-like chain in the absence of any fluid are presented. Such a study is not feasible at present for realistic models of proteins, so simplified models are used to capture the basic behavior of proteins. Discontinuous potentials are used for the interaction potentials, where attraction and repulsion are defined as step and shoulder potentials respectively. The Hybrid Monte Carlo (HMC) method¹² is applied for the sampling of the energy landscape of a protein-like chain in which the Monte Carlo sampling is done using parallel tempering (PT) and the generation of trial configurations is carried out by discontinuous molecular dynamics (DMD). The PT method^{13–15} improves the convergence properties of Monte Carlo sampling by decreasing the correlation length of samples in the Markov chain of states¹⁶.

It is shown that for two simple protein models, each consisting of a periodic sequence of four different kinds of bead, the folded state exhibits a secondary alpha helix structure. It is demonstrated that the relative configurational entropies of the protein-like chains are independent of temperature for the discontinuous potential models, which makes it possible to compute the relative configurational entropies and the free energies of the configu-

rations very accurately. Relative configurational free energies at different temperatures can be determined from relative populations at those temperatures. The free energy results can be interpreted in terms of the free energy landscape picture. Such understanding of the free energy landscape is the main objective of this work.

In Sec. II the models and their parameters are described, and it is shown that relative configurational entropies are temperature independent in the models. A simplified three state model is also presented to facilitate the interpretation of the simulation results. In Sec. III, the results for the observed structures, configurational entropy and free energy differences are presented, and the shape of the free energy landscape is analyzed both for short and long chains. Conclusions are given in Sec. IV.

II. MODELS OF THE PROTEIN-LIKE CHAIN

In this article we consider a *beads on a string* model of a protein-like chain in which each bead represents an amino acid or residue. The chain consists of a repeated sequence of four different kinds of beads. While having four different types of beads is not enough to represent the twenty different types of amino acids, it preserves at least some of the differences between amino acids. The interactions between these beads are designed to mimic the interactions that lead to the formation of common motifs in protein structure, such as the alpha helix. Previous studies suggest that chains containing only 6, 8 or 12 monomers are too short to fold into compact states at low temperatures, while somewhat longer chains with 25 monomers can capture folded helical states¹⁷. Here, chains of moderate lengths of 15 to 35 beads have been used to facilitate the exploration of the free energy landscape.

The models analyzed here allow for attractive interactions, intended to mimic hydrogen bonds between non-adjacent residues, between beads separated from each other by $4n$ beads, where $n \geq 1$, and with additional restrictions on the possible hydrogen bonds to be specified below. Several versions of the models of protein-like chains have been considered, but only the results for two of them are presented here. Models were selected based on the similarity of preferred structures in the model to those observed in real proteins.

To make contact with real proteins, physical units are used in the definition of the model, although these should not be taken too literally. In particular, lengths will be expressed in Ångströms, energies in kJ/mol and masses in atomic mass units.

The two models analyzed here differ in the hydrogen-bond potentials, while other interactions are the same. In total, four different potentials are used in these models. The first kind of potential acts between the nearest and the next nearest neighbors and restricts the distance between the beads to specific ranges by applying an infinite square-well potential similar to Bellemans' bonds

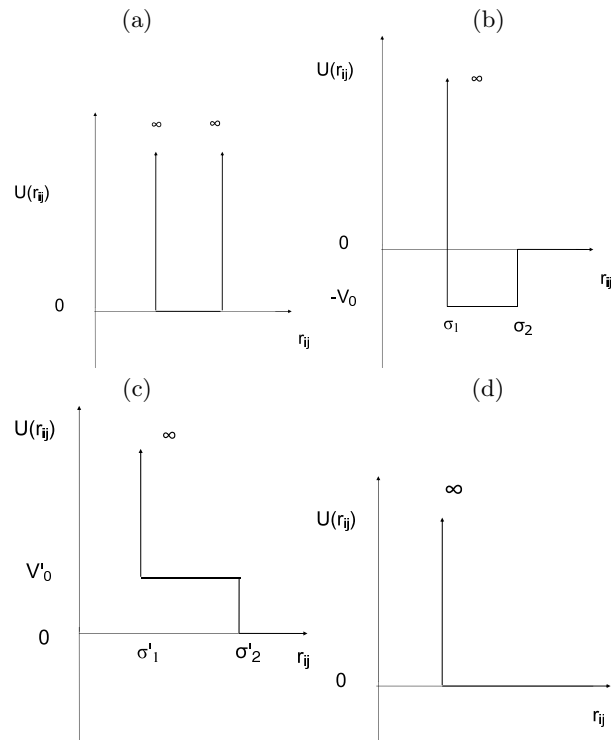


FIG. 1: Model potentials: the (a) infinite square-well potential, (b) attractive step potential, (c) repulsive shoulder potentials, and (d) hard core repulsion.

model¹⁸. Fig. 1(a) shows the shape of this kind of potential. To mimic a covalent bond between two consecutive amino acids in the protein, the distance between two neighboring beads is restricted to the range 3.84 Å to 4.48 Å. This potential allows these distances to vibrate around values close to the distance between stereocenters used in Ref. 19. Bond angle vibrations are similarly represented by defining infinite square-well potentials between next-nearest neighbors in the chain. Restricting their distance to a range from 5.44 Å to 6.40 Å generates a vibration angle between 75° and 112°. For simplicity, dihedral angles are not considered in our models, but as discussed later, some restrictions on hydrogen bonds are employed to create rigidity in the backbone of the protein-like chain similar to the rigidity that results from the dihedral angle interactions in more detailed potentials.

Hydrogen bonds are modeled by an attractive square-well potential, depicted in Fig. 1(b). In all models investigated here, the attractive forces are defined between beads i and $i + 4n$ (with n integer) to resemble the hydrogen bonds in alpha helix structures. However, the two models differ in the possibility of these attractive bonds and the values of i and n .

In the first model, named model A, the attractive interactions act between half the same type beads such that bonds can be formed between two beads both with an index of the form $i = 4k + 1$, or both with an index of

the form $i = 4k + 3$, where k is an integer number.

In the second model, model B, only the beads with index $i = 4k + 2$ can bond with each other, and n cannot be 2 or 3. This means that there is no attractive bond between beads separated along the chain by eight or twelve beads. Bonds between beads i and $i + 8$ as well as i and $i + 12$ are disallowed to make the occurrence of turns more difficult in the protein-like chain and effectively make it more rigid. This restriction has a similar function to torsional interaction potentials defined in terms of dihedral angles along the backbone of the chain in more detailed models where they prevent a protein from bending over easily. In Fig. 2 the possible attractive bonds for the two models are presented for a chain of length 25 in which subsequent beads were labeled A through Y. It will be shown that the two models have different thermodynamic characteristics and important qualitative differences in their free energy landscape due to the difference in the hydrogen bonding interactions.

For both models, the parameters for the attractive square-well potential, σ_1 and σ_2 , are chosen to be 4.64 Å and 5.76 Å with a mid point of 5.2 Å, which is close to the translation of 5.4 Å along each turn of an alpha helix. Compared to covalent bonds, these attractive interactions act across longer distances. The depth of the potential well ϵ is 20 kJ/mol and the mass of each bead is set to 2×10^{-25} kg, which is close to 120 atomic mass units.

To represent electrostatic interactions of the atoms, repulsive interactions act between beads $1 + 4k$ and $4k'$, where k and k' are integers and $k \neq k'$. The repulsive interaction takes the form of a shoulder potential, shown in Fig. 1(c). The range of the shoulder is set to be from 4.64 Å to 7.36 Å, while the height is 0.9ϵ . The effect of changing the number of step repulsions in a few models was evaluated in terms of minimizing the free energy. It turned out that changing the number of repulsions does not have a huge impact on the shape of free energy landscape around the native structure point. Since the repulsion between the beads increases the potential energy while decreasing the configurational entropy, the most common structures at low temperatures do not have any repulsive interactions. Therefore, the two models differ only in their attractive potentials, while their repulsive interactions are the same.

Finally, all other bead pairs for which no covalent bonds, hydrogen bonds or shoulder repulsive interactions are defined interact via a hard sphere repulsion to account for excluded volume interactions at short distances, depicted in Fig. 1(d). The hard sphere diameter is set to be 4.64 Å, which is slightly different from the value of 4.27 Å used by Zhou et al.¹⁹.

The reduced temperature is defined as $T^* = (k_b T)/\epsilon$, where ϵ is the potential depth of the square-well attractive interactions, and β^* is the inverse of the reduced temperature, $\beta^* = 1/T^*$. Given the value of $\epsilon = 20$ kJ/mol, $T^* = 1.0$ corresponds to 2400 K. This means that $\beta^* = 8$ ($T^* = \frac{1}{8}$) roughly corresponds to standard room temperature, 300 K.

A. Definition of configurations

One of the advantages of using discontinuous potentials is the ease of comparing configurations. The bonds are defined using the specific range of bead separations r_{ij} in which the potential energy $V = \frac{1}{2} \sum_{ij} U(r_{ij})$ is equal to a specific, non-zero value. Since only one attractive bond can exist between each bead pair (i, j) in the current models, each configuration or structure can be represented by a matrix of interactions in which the entry at row i and column j is unity if i and j are bonded and zero otherwise. Because bonded interactions largely determine the form of the protein, this matrix can be used to identify the configuration of the protein-like chain. Thus, by comparing the matrices, identical structures can be easily found.

However, for ease of presentation, a more readable alphabetical notation for configurations is applied. Each bead is represented by a subsequent letter from the alphabet and each bonded interaction is shown by a pair of letters. The two dimensional matrix can thus be represented by a string of alphabetical pairs. Since most of the studied cases involve 25-bead chains, A to Y have been used to label different beads. For chains longer than 26 beads, both capital and small letters can be used.

B. Temperature independence of relative configurational entropies

The definition of configurations presented above was based on the presence of attractive bond interactions. Within the model, having a certain set of bonds (and no others) leads to a specific potential energy U_c for each configuration c . As shown below, this leads to a temperature independent relative configurational entropy.

The configurational entropy of any particular configuration c is the entropy of a sub-ensemble in which the phase points are restricted to those of configuration c . The discrete nature of the interactions allows configurational space to be partitioned into microstates by defining an index function for a configuration c that depends on the set of spatial coordinates of the chain \mathbf{R}

$$\chi_c(\mathbf{R}) = \begin{cases} 1 & \text{if only bonds in } c \text{ are present,} \\ 0 & \text{otherwise.} \end{cases}$$

The partitioning of configurational space arises naturally by expanding the product in the identity

$$1 = \prod_{i=1}^{n_b} (1 - H(x_i - \sigma_2) + H(x_i - \sigma_2))$$

$$= \prod_{i=1}^{n_b} (H(\sigma_2 - x_i) + H(x_i - \sigma_2)) \quad (1)$$

$$= \sum_{k=1}^{n_s} \chi_{c_k}(\mathbf{R}), \quad (2)$$

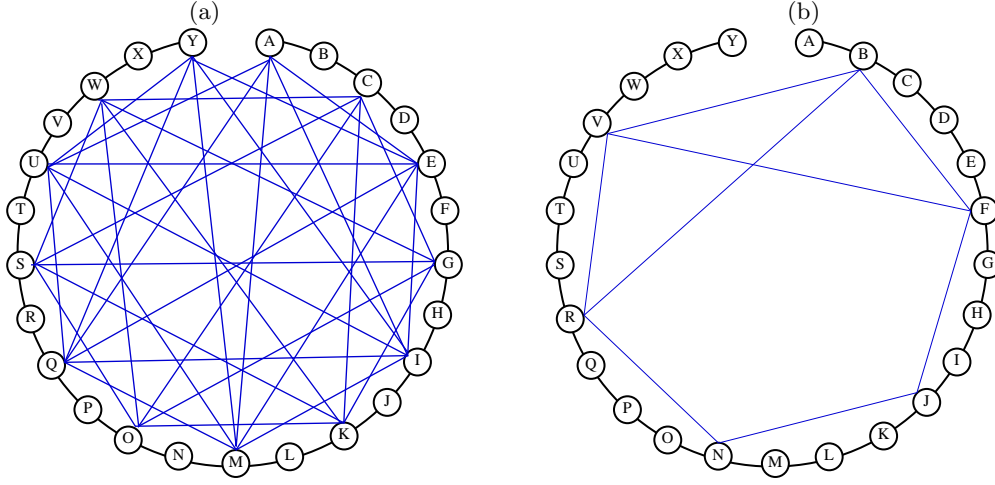


FIG. 2: Possible attractive bonds of (a) model A, and (b) model B for a chain of 25 beads.

where n_b is the number of attractive bonds in the model, $n_s = 2^{n_b}$ is the number of microstates, and $H(x)$ is the Heaviside function

$$H(x) = \begin{cases} 1 & x \geq 0 \\ 0 & \text{otherwise.} \end{cases}$$

In Eq. (2), x_i is the distance between monomers in the i th bond, and σ_2 is the critical distance at which an attractive hydrogen bond is formed. For notational simplicity, we order the index of configurations based on the number of bonds starting with the configuration with no bonds, $\chi_1(\mathbf{R}) = \prod_{i=1}^{n_b} H(x_i - \sigma_2)$, and ending with the configuration with the maximum number of bonds, $\chi_{n_s}(\mathbf{R}) = \prod_{i=1}^{n_b} H(\sigma_2 - x_i)$.

In the canonical ensemble, the probability $f_{\text{obs}}(c, T)$ of observing a configuration c at temperature T is

$$f_{\text{obs},c} = e^{-\beta(F_c - F)}, \quad (3)$$

where F_c is the free energy of configuration C , and F is the full free energy of the system. By definition, one has

$$e^{-\beta F_c} = \frac{1}{h^{3N}} \int dR dP \chi_c(R) e^{-\beta \left[\sum_{i=1}^N \frac{|p_i|^2}{2m} + V(R) \right]}, \quad (4)$$

where N is the number of beads, m is their mass, and V is the potential energy function. The configurational entropy is related to F_c via

$$F_c = E_c - TS_c, \quad (5)$$

where E_c is the average energy of configuration c at temperature T . Since its potential energy V is always equal to U_c when it is finite and $\chi_c = 1$, one has

$$E_c = U_c + \frac{3}{2} N k_B T. \quad (6)$$

Combining Eqs. (4)-(6), one finds

$$S_c = \frac{3}{2} N k_B \ln \left(\frac{2\pi m e}{\beta h^2} \right) + k_B \ln \int' dR \chi_c(R), \quad (7)$$

where the integral is restricted to sum over configurations that satisfy all geometric constraints due to the infinite square-well and hard core repulsions. Thus the *relative* entropy of two configurations c_1 and c_2 at a specific temperature is

$$\Delta S_{c_1 c_2} = S_{c_1} - S_{c_2} = k_B \ln \frac{\int' dR \chi_{c_1}(R)}{\int' dR \chi_{c_2}(R)}, \quad (8)$$

which does not depend on temperature.

From Eqs. (6) and (7) it can be concluded that the free energy of a configuration is

$$F_c = U_c - \frac{3}{2} N k_B T \ln \left(\frac{2\pi m}{\beta h^2} \right) - k_B T \ln \int' dR \chi_c(R), \quad (9)$$

where the second term is the same for all the configurations at temperature T .

Because relative configurational entropies do not depend on temperature, relative entropies can be determined from a single run at a temperature T , using

$$\begin{aligned} \Delta S_{c_1 c_2} &= \frac{\Delta E_{c_1 c_2} - \Delta F_{c_1 c_2}}{T} \\ &= \frac{\Delta E_{c_1 c_2}}{T} + k_B \ln \frac{f_{\text{obs}}(c_1, T)}{f_{\text{obs}}(c_2, T)} \end{aligned} \quad (10)$$

$$= \frac{\Delta U_{c_1 c_2}}{T} + k_B \ln \frac{f_{\text{obs}}(c_1, T)}{f_{\text{obs}}(c_2, T)}. \quad (11)$$

Therefore, no approximation is necessary to calculate the relative configurational entropies in contrast to molecular dynamics (MD) studies utilizing smooth potentials (see e.g. Ref. 20).

C. Simulation Techniques

The simulation results presented here were obtained utilizing a sampling method that uses a combination of

dynamical updates based on DMD and PT exchange moves. In this approach, a number of replicas are updated simultaneously using molecular dynamics (appropriate for the discontinuous potential systems²¹) for a fixed amount of time. At the start of a dynamical update, the velocities of all beads in the chain are drawn from the Maxwell-Boltzmann distribution for each replica at the temperature appropriate for that replica. Since the DMD is time-reversible, exactly conserves energy and preserves phase space volume²², the limit distribution of the Markov chain of states for each replica is canonical at the temperature of the Markov chain¹². Furthermore since the total energy is conserved exactly in the dynamics, the updates provide a rejection-free means of moving all degrees of freedom simultaneously. To enhance the sampling efficiency, the dynamical updates are combined with replica exchange updates. The replica exchange moves are designed so that the states at each temperature are canonically distributed^{13,14}. The process of drawing velocities, DMD dynamics, and PT exchange moves is repeated until enough independent statistics on the frequency at which different configurations are seen is gathered.

D. Simplified three state model

In the simulations, one can easily measure the frequency of occurrence $f_{\text{obs}}(c)$ of configurations c at each temperature in the PT replica set. The accuracy of $f_{\text{obs}}(c)$ is $\mathcal{O}(\sqrt{f_{\text{obs}}(c)})$, and thus is highest for the most frequently occurring (dominant) structure. For that reason, below, we will often plot the observed frequency f^* of the most common structure, i.e. $f^* = \max_c f_{\text{obs}}(c)$, as a function of the inverse temperature β . To facilitate the interpretation of such a plot, it is helpful to consider

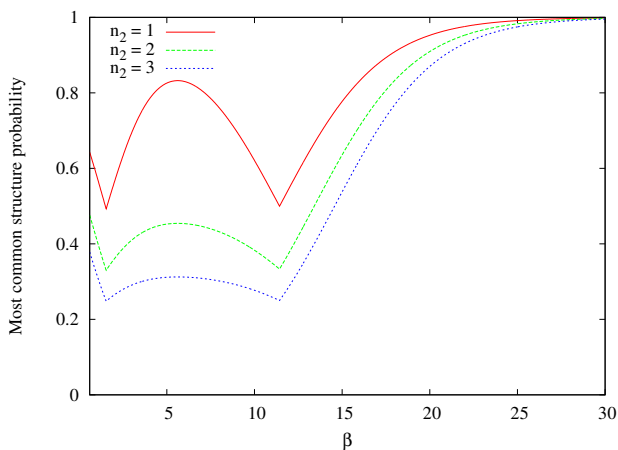


FIG. 3: Variation of the probabilities of the most common structure versus the inverse temperature for the three state model with parameters $E_2 = -0.65$, $S_2 = 4$, $S_3 = 5$, and three different values for n_2 .

its form for the following, simplified three-state model. The three states are configurations with energies E_1 , E_2 and E_3 , and entropies S_1 , S_2 , and S_3 , respectively. As in the actual model of the protein-like chain, the values of entropies do not depend on temperature. The second state will furthermore be taken to be n fold degenerate (this is thus really a $n + 2$ state model).

For each state in this model, the observational frequency is

$$f_{\text{obs}}(c, \beta) = \frac{e^{-\beta E_c + S_c/k_B}}{Z(\beta)}, \quad (12)$$

where c ranges from 1 to 3 and

$$Z(\beta) = e^{-\beta E_1 + S_1/k_B} + n e^{-\beta E_2 + S_2/k_B} + e^{-\beta E_3 + S_3/k_B} \quad (13)$$

We will assume that $E_1 < E_2 < E_3$ and $S_1 < S_2 < S_3$, such that configuration 1 models the native state with lowest energy and lowest entropy, configuration 3 models the unfolded state with high energy and high entropy, while configuration(s) 2 can be interpreted as intermediate. Because only relative energies and entropies affect f^* , we can set E_3 and S_1 to zero. Furthermore, one can fix the temperature scale by setting E_1 to -1 . That leaves just four parameters in the model: n_2 , E_2 , S_2 and S_3 (subject to the constraint that $S_2 < S_3$).

Figure 3 shows three examples of the behavior of f^* for this model, corresponding to the following choices of the parameters: $E_2 = -0.65$, $S_2 = 4$, $S_3 = 5$, and $n_2 = 1$, 2, and 3, respectively. One sees a ‘bouncing’ signal as subsequent states become dominant when temperature is varied. There are cusp-shaped minima where the identity of the dominant state changes. At that point, several configurations are equally likely. If one neglects the other, non-dominant, configurations at that point, then the value of f^* at a cusp should be one over the number of competing structures, and this is borne out by the plots shown in Fig. 3, which show cusp depths close to $1/2$, $1/3$ and $1/4$, respectively. As β increases (temperature gets lower), the frequency of observing state 1 (the ‘native’ state) reaching almost 100%.

One can expect similar results for the protein-like chain model used in the simulations. The main difference with the three-state model is the presence of many more configurations. Some of these extra states will be irrelevant (have negligible f_{obs}) because of their low entropy, but one could expect to see extra bounces in the plots for the real model from some additional relevant states.

III. RESULTS

A. Free energy landscape

To characterize the (free) energy landscape at a specific temperature, the most common structures are identified and their relative free energies computed at that temperature. Two structures are close in the landscape if they

β^*	the most common structure	$f_{\text{obs}}(\%)$
1.5	No bond	14.2 \pm 0.6
14.0	AE AI AY CG CK CS CW EI GK GO GS IY KO KS KW MQ MU OS QU SW	9.7 \pm 0.6
24.0	AE AI AY CG CK CS CW EI GK GO GS IY KO KS KW MQ MU OS QU SW	10.6 \pm 0.6
38.4	AQ AU AY CG CO CS CW EI EM GK GO GS GW IM KO KS OS QU SW UY	8.5 \pm 0.6
57.5	AQ AU AY CG CO CS CW EI EM GK GO GS GW IM KO KS OS QU SW UY	7.7 \pm 0.6
72.5	AE AI AM CG CK CO CS EI GK GS GW KO KS KW OS OW QU QY SW UY	8.1 \pm 0.6
87.5	AE AI AM AQ AU AY CG CK EI EY GK IM IQ IY MQ MU OS QU QY SW UY	8.2 \pm 0.6
β^*	the second most common structure	$f_{\text{obs}}(\%)$
1.5	SW	2.1 \pm 0.2
14.0	AE AI AY CG CK CO CS CW EI GK GO IY KO KW MQ MU OS OW QU SW	8.7 \pm 0.6
24.0	AE AI AY CG CK CO CS CW EI GK GO IY KO KW MQ MU OS OW QU SW	9.6 \pm 0.6
38.4	AE AI AY CG CK CO CS CW EI GK GO IY KO KW MQ MU OS OW QU SW	6.6 \pm 0.4
57.5	AE AI AM CG CK CO CS EI GK GS GW KO KS KW OS OW QU QY SW UY	4.5 \pm 0.4
72.5	AQ AU AY CG CO CS CW EI EM GK GO GS GW IM KO KS OS QU SW UY	7.5 \pm 0.4
87.5	AE AU AY CG CS CW EY GK GS GW IM IQ KO KS KW MQ OS OW SW UY	6.6 \pm 0.6

TABLE I: Most common configurations of the model A 25-bead chain.

β^*	the most common structure	$f_{\text{obs}}(\%)$
1.5	No bond	22.4 \pm 1.2
3.0	No bond	6.7 \pm 1.0
3.5	BF JN	4.0 \pm 0.6
4.2	BF FJ NR RV	6.5 \pm 0.8
4.5	BF BR BV FJ FV JN NR RV	7.5 \pm 1.0
5.3	BF BR BV FJ FV JN NR RV	46.4 \pm 1.6
6.0	BF BR BV FJ FV JN NR RV	76.0 \pm 1.2
7.5	BF BR BV FJ FV JN NR RV	94.1 \pm 0.8
13.5	BF BR BV FJ FV JN NR RV	99.9 \pm 0.0
β^*	the second most common	$f_{\text{obs}}(\%)$
1.5	BF	3.5 \pm 0.6
3.0	BF	5.6 \pm 0.8
3.5	BF NR	4.0 \pm 0.6
4.2	BF FJ JN RV	4.9 \pm 0.8
4.5	BF FJ JN NR RV	6.4 \pm 0.8
5.3	BF BR BV FJ JN NR RV	10.1 \pm 0.8
6.0	BF BR BV FJ JN NR RV	6.8 \pm 0.8
7.5	BF BR BV FJ JN NR RV	1.9 \pm 0.6
13.5	N/A	N/A

TABLE II: Most common configurations of the model B 25-bead chain.

have similar configurations, which means that they have a large number of bonds in common. For model A, the dominant structures are shown in Table I, while those for model B are given in Table II, both for a chain length of 25. The dominant structures at low temperatures are designed to be helical in nature, with long chains allowing for a primitive tertiary structure in which the helix folds back on itself (see Fig. 4). The most common structures at any temperature are those with the lowest Helmholtz free energy at that temperature. Therefore,

at low enough temperatures, when the effect of entropy is small, the most common structure is the one with the lowest possible potential energy, which will only have attractive bonds and no repulsive bonds. Therefore, unless otherwise specified, here the term “bond” refers only to an attractive bond (or hydrogen bond) and not repulsive or covalent bonds. Using their interaction matrices, it is relatively easy to count the number of occurrences of the different structures and to find the most common structures.

According to the diagram in Fig. 2(b), for model B, the maximum number of attractive bonds is 8 for the 25-bead chain. As expected, the most common structure for model B at low temperatures, $\beta^* \geq 4.5$, has 8 attractive bonds (cf. Table II) and therefore has the lowest potential energy for this model. According to Table I, the lowest potential energy configuration in model A for the 25-bead chain has 21 attractive bonds. However, according to Fig. 2(a), 36 possible attractive bonds are available for the 25-bead chain in model A. This means that either the configurations with lower energies that have more than 21 attractive bonds are not geometrically accessible (due to constraints in the model) or their configurational entropies are too low to be observed at these temperatures. It will be shown later (Sec. III D) that the former scenario is the case. However, if the latter scenario were true, the lower energy configurations would become dominant by reaching lower temperatures.

Within the framework of the model, a folding funnel is identified as a region of phase space points corresponding to a set of configurations from which the folded structure is easily and rapidly accessible as the temperature is lowered. This means that the barriers between local minima located inside the funnel, such as those arising from entropic decreases associated with the formation of new bonds, are small. As the temperature is lowered, new minima appear in the funnel region of the energy land-

scape, corresponding to nearby configurations that differ in relatively few bonds from the previously favored structures. If barriers between nearby states in the landscape are small, the system rapidly equilibrates to the presence of new minima and adopts a more folded structure. Although the specific pathway through which the system folds may involve a number of intermediate structures, the intermediate structures emerge smoothly with temperature and provide a channel to the folded structure.

A quantitative measure of the folding funnel can be obtained by examining how the dominance f^* of the most preferred structure changes with temperature, where f^* is the probability of observing the most common configuration. For real protein systems in which a single, folded structure is thermodynamically stable, one expects that f^* is near unity for temperatures at which the protein is folded. Furthermore, if the protein folds readily as the inverse temperature β increases, then we expect $df^*/d\beta$ to be large and positive in the vicinity of the inverse folding temperature.

As can be seen in Table I, by decreasing the temperature for model A, some dominant structures are observed, but by decreasing the temperature further, the ratios of their populations to the total population starts to decrease and new structures become dominant. It can be concluded that in this model, the shape of the landscape changes significantly by varying the temperature, where at high temperatures the landscape is riddled with many local minima (many equally preferred structures) and one very deep but wide minimum (no bonded structure), and at low temperatures there are a few narrow deep minima. For model A, either there are deep local minima inside a funnel shaped valley or there are only a few deep local minima beside each other. At the studied temperatures, there is no structure with a very large population, which confirms that there is deep global minimum in the free energy landscape. Since the most common structures at each temperature differ from each other in a few bonds, these deep minima are located close to each other in the landscape but not inside a funnel in the sense that they are not structures that are adjacent in the configurational space and can only be converted into one another through intermediates. The barriers involved in these conversions are high enough to make this a slow process. For example, as can be seen in Table I, the first two most common structures at $\beta^* = 57.5$ differ in seven bonds. Hence there are many barriers that must be overcome to go between the two configurations because seven bonds must be broken and seven new bonds must be formed. On the other hand these two structures share thirteen bonds (65% of their total bonds), which indicates that they are similar and therefore their locations in the landscape are still relatively close to each other.

Unlike the behavior observed in model A, a single dominant structure is identified in model B by decreasing the temperature, where the probability f^* of the most common structure attains a value of nearly one at low temperatures (See Table II). For $\beta^* \geq 5.3$, the free en-

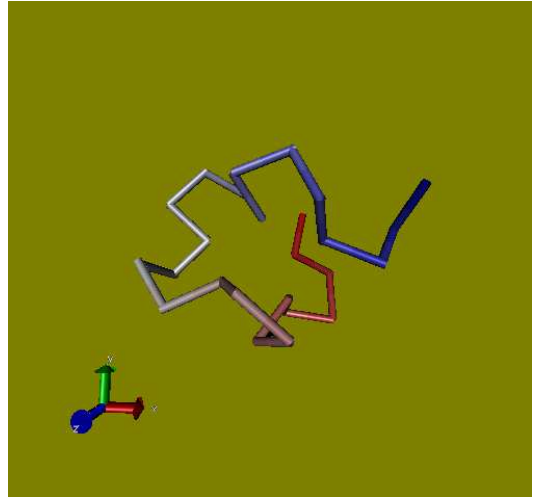


FIG. 4: Folded helical structure for model B with 8 bonds.

ergy landscape consists of a single channel in which there are several minima. The most common structures for $\beta^* = 6$ are presented in Table III. None of the seven most common structures have a repulsive bond. This is not surprising, since the formation of a repulsive bond both limits the number of accessible conformations and is energetically unfavorable. The most common structure for $\beta^* \geq 5.3$, BF BR BV FJ FV JN NR RV, is the deepest point in the funnel, and the six other most common structures listed in Table III differ only in one bond from this structure. This means that there is a funnel-shaped valley with a global minimum corresponding to a folded helix and there are a few local minima of higher free energy beside this deepest point of the landscape. According to Table II, by lowering the temperature the deepest point of the funnel becomes deeper while the other minima become shallower, since the population of the most common structure reaches a value higher than 99.9%. This implies that the funnel becomes smoother and steeper as the temperature decreases, and the lowest free energy configuration becomes more accessible.

The variation of the probability of the most common structure f^* for the two models as a function of temperature is shown in Fig. 5 for chains of 25 beads. For both models, there is a cusp-shaped minimum at which a low-

Rank	most common structure	$f_{\text{obs}}(\%)$
1	BF BR BV FJ FV JN NR RV	76.0 ± 1.2
2	BF BR BV FJ JN NR RV	6.8 ± 0.8
3	BF BV FJ FV JN NR RV	3.8 ± 0.6
4	BF BR BV FV JN NR RV	1.9 ± 0.4
5	BF BR BV FJ FV JN RV	1.3 ± 0.4
6	BF BR BV FJ FV NR RV	1.0 ± 0.3
7	BF BR BV FJ FV JN NR	1.0 ± 0.3

TABLE III: Most common configurations of the model B 25-bead chain at $\beta^* = 6$.

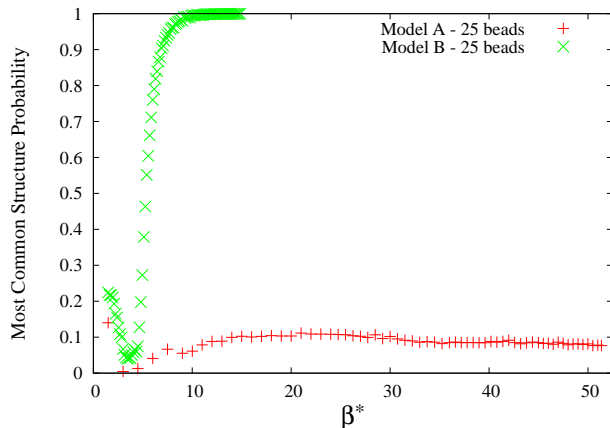


FIG. 5: Variation of the probabilities of the most common structure f^* versus the dimensionless inverse temperature β^* for chains with 25 beads.

energy structure becomes dominant. The value of the probability is very low at the minimum, indicating many competing structures (see Sec. IID). For model A, the probability of the most common structure at low temperatures is fluctuating around a small value of about 0.08, whereas for model B, the probability of the most common structure nearly attains unity. This demonstrates once more that the free energy landscape for model A does not have a funnel-like shape.

It will become clear in Sec. IIID that even for model B, the funnel-like character of the free energy landscape does not persist for chains longer than 29 beads due to geometric frustration.

	configuration	U_c/ϵ	S_c/k_B
1	AD	0.9	31.3 ± 0.8
2	No Bond	0.00	31.8 ± 0.6
3	BF	-1	28.6 ± 0.6
4	BF JN	-2	25.1 ± 0.6
5	BF NR	-2	25.2 ± 0.6
6	BF JN RV	-3	21.7 ± 0.4
7	BF FJ NR RV	-4	17.8 ± 0.6
8	BF FJ JN RV	-4	17.6 ± 0.6
9	BF FJ JN NR RV	-5	13.2 ± 0.6
10	BF BR BV FJ JN NR RV	-7	3.7 ± 0.8
11	BF BV FJ FV JN NR RV	-7	2.9 ± 0.6
12	BF BR BV FJ FV JN NR RV	-8	0

TABLE IV: Potential energy in units of ϵ and relative entropy of the most common structures of the model B 25-bead chain.

B. Entropy and free energy calculation for the 25-bead chain in model B

As discussed in Sec. IIB, and as expressed in Eq. (11), the relative configurational entropies and consequently the free energy difference of two configurations can be obtained from the ratio of their probabilities at a specific temperature. Since there are fewer possible structures in model B than in model A, the statistical uncertainty in the populations, and therefore also in the entropies and free energies, is smaller for model B. For this reason, and because it is already clear that model A does not have a funnel-like free energy landscape, subsequent analysis will focus on the characteristics of model B.

The value of the entropy of a configuration should depend largely on the number of bonds that it has, since the formation of a bond restricts the distance between a specific pair of beads. As can be seen in Table IV, although the entropies of configurations with the same number of bonds differ slightly, they are similar in magnitude. Typically, the entropy decreases by increasing the number of bonds due to additional geometric constraints, with the entropy loss typically on the order of $3k_B$ per bond. Nonetheless, one sees that configurations with the same energy of -6ϵ have somewhat different populations and therefore different entropies.

Although in principle, the entropy difference between any two configurations can be calculated based on the ratio of their populations, often there is little overlap between the population distributions of the most common structure at very low temperatures and the most common structure at very high temperatures (e.g., configurations 2 and 12 of Table IV). Since the configurational entropy difference is independent of temperature, this difficulty is easily overcome by using one or two intermediate configurations whose population distribution do have sufficient overlap at some range of temperatures. Using the calculated entropies, one can compute the relative Helmholtz free energy between any pair of configurations at any temperature. This allows one to predict the population

β^*	configuration	p_{pred}	f_{obs}	$\Delta(\%)$
1.5	No Bond	0.206	0.165	25
1.5	BF	0.068	0.059	15
1.5	RV	0.059	0.065	9
5.0	BF BR BV FJ FV JN NR RV	0.949	0.941	0.8
5.0	BF BR BV FJ JN NR RV	0.020	0.019	5
5.0	BF BV FJ FV JN NR RV	0.010	0.012	17
6.0	BF BR BV FJ FV JN NR RV	0.988	0.980	0.8
6.0	BF BR BV FJ JN NR RV	0.005	0.005	0
9.0	BF BR BV FJ FV JN NR RV	0.999	0.999	0

TABLE V: Comparison of the predicted probability (p_{pred}) and the simulation results for the frequency (f_{obs}), and their relative difference (Δ), for the most common structures of the model B 25-bead.

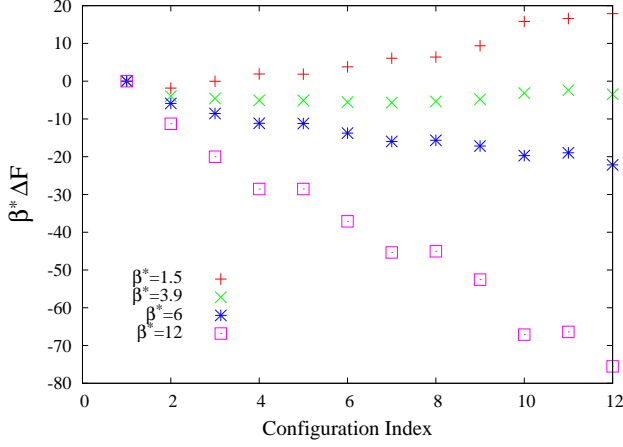


FIG. 6: Variation of $\beta^* \Delta F$ versus the configuration index of Table IV for model B, where ΔF is the Helmholtz free energy difference with configuration 1 in unit of ϵ .

of any structure at any temperature and predict the temperature at which the population of two specific configurations becomes equal. The free energy and entropy of some of the most common structures of model B for the 25-bead chain are shown in Table IV.

The variation of $\beta^* \Delta F$ versus the configuration index of Table IV — which one could view as a simple way to plot the free energy landscape — is shown in Fig. 6. The zero-point of this free energy plot was (arbitrarily) chosen to be the free energy of configuration 1 (AD), i.e., free energies were computed as $\Delta F_{1c} = U_c - TS_c - (U_1 - TS_1)$, where U_c and S_c were taken from Table IV. Since both the entropy and the energy of the configurations are decreasing from configuration 1 to 12, the behavior of $\beta^* \Delta F$ is very different for high and low temperatures. At high temperatures ($\beta^* \leq 3$), entropy effects dominate, and the configuration with the largest entropy in Table IV (configuration 2) is the lowest free energy structure for $\beta^* = 1.5$ in Fig. 6. Note that the free energy of other structures increases with increasing number of attractive bonds. In contrast, at lower temperatures, energy effects dominate the free energy landscape, and indeed, in Fig. 6, the configuration from Table IV, which has the lowest potential energy, is seen to be the lowest free energy structure for $\beta^* = 6$ and $\beta^* = 12$.

Using the values in Table IV, one can determine that for $\beta^* \geq 4.5$, the folded helix configuration (configuration 12) becomes dominant, since for all the temperatures in that range, this configuration has the lowest free energy. The simulation results for the population of each configuration confirm this prediction. When configurations are ranked according to their populations, configuration 12 ranks 30th, 13th and 5th for β^* values of 4.05, 4.2 and 4.35 respectively, while for $\beta^* \geq 4.5$, it ranks first place.

The relative free energy of configurations 2 and 12 is plotted against β^* in Fig. 7. It can be seen that at $\beta^* \approx 4$ their free energies are equal, which implies that their populations are the same. Indeed, simulation results indicate

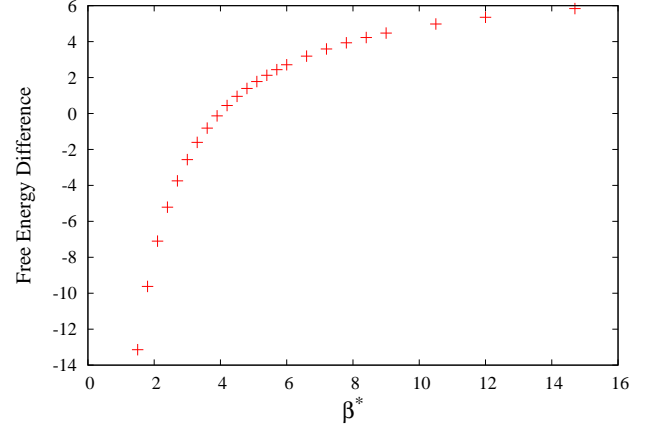


FIG. 7: Temperature dependence of the free energy difference of configurations 2 and 12 of 25-bead model B, as listed in Table IV, in units of ϵ .

that the populations of configuration 2 and configuration 12 at $\beta^* = 3.9$ are 1.0% and 0.5%, respectively and at $\beta^* = 4.05$ are 0.6% and 1.2%, respectively, which confirms that their population should become equal in the range $3.9 \leq \beta^* \leq 4.05$.

It should be noted that in our calculations, structures that have a population of less than 0.5% are not considered to simplify computations. As a result, when calculating the probabilities of the configurations with 25 beads, only 78 configurations were used. Although this introduces a systematic error, the predicted probabilities are very close to the observed ones from the simulation runs, as can be seen in Table V. According to this table, the predicted values agree better with the simulation results at lower temperatures. The disagreement is due to the fact that some configurations with very low populations have not been considered in the probability calculations, but since these configurations occur more frequently at high temperatures, neglecting their contribution leads to a larger error at high temperatures.

C. Entropy and free energy calculation for the 35-bead model B chain

The entropies and free energies of 35-bead configurations are calculated in a similar way to the 25-bead case. Adding only 10 beads to the chain changes the number of possible attractive bonds from 8 in the 25-bead chain to 23 in the 35-bead chain (cf. 2), which results in a much more complex energy landscape.

The dramatic change in landscape can be seen in Table VI and Fig. 9, where we see that, unlike the 25-bead chain, the probability of the most common structure does not approach unity even at very low temperatures.

As can be seen in Table VI, by increasing β^* (decreasing temperature) a few structures become dominant at different temperatures. Except for the lowest energy con-

figuration with 23 attractive bonds, other energies are degenerate with multiple configurations possessing the same number of bonds. It will be shown in the next section that a structure with 23 attractive bonds is geometrically prohibited. In fact, configurations with 21, 22, or 23 attractive bonds have not been observed in any simulation runs.

One difference between the landscape of the 35-bead chain and that of the 25-bead chain is the magnitude of the entropic barriers between configurations with different energies. The most common structures in Table VI at high β^* have an energy of -19ϵ . Beside the two main configurations with the energy of -19ϵ , which are presented in Table VI, there are at least 18 other configurations with the same potential energy but with lower entropies. Three structures with an energy of -20ϵ and with relatively low entropies have been observed in the runs as well, but, according to Table VI, these were never among the first two most common structures. The configuration with the potential energy of -20ϵ that has the highest entropy is different in five bonds from the most common configuration of Table VI. This implies that there is a substantial entropic barrier between these configurations.

A second difference with the 25-bead case is that a few different configurations of the 35-bead chain exist at low temperatures and are observed with nearly the same frequency. For example, as Table VI shows, the two most common structures for $16.5 \leq \beta^* \leq 53$ have 19 attractive bonds. While these two structures differ slightly in their populations, structurally they differ by more than one bond, quite unlike the seven most common structures of the 25-bead chain at $\beta^* = 6$ (cf. Fig. III) which only differ from each other by one bond. Since the most common structures of the 35-bead chain at low temperatures share most of their bonds, they are near one another in the energy landscape. However, since the most common structure differs from other common structures by more than one bond, they do not necessarily lie inside a single valley in the landscape. A more plausible interpretation is that the landscape at low temperatures for the 35-bead chain consists of several minima that are close but not necessarily inside the same channel, and that the landscape does not have a single deep minimum at very low temperatures.

A final difference with the 25-bead case that becomes apparent is that the range of energies and that of entropies for the observed configurations are 8ϵ and $32k_B$ respectively for 25-bead chains, while these are 20ϵ and $140k_B$ respectively for 35-bead chains. This confirms the view that the landscape of the 35-bead chain is much wider than the 25-bead chain landscape. This also shows that studying the landscape requires a much wider range of temperatures and more replicas.

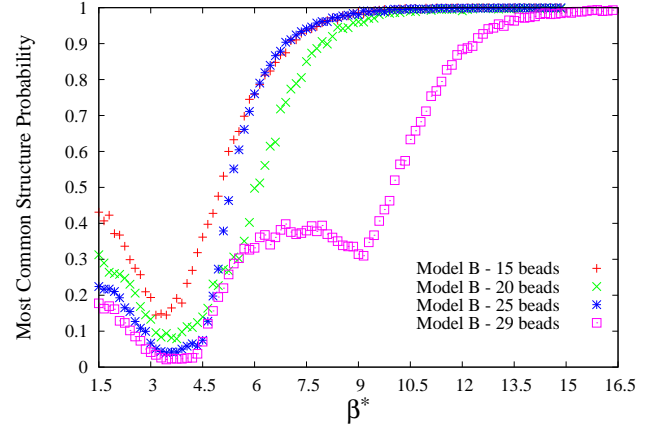


FIG. 8: Variation of the probabilities of the most common structure, f^* , versus the β^* for chains with 15, 20, 25 and 29 beads

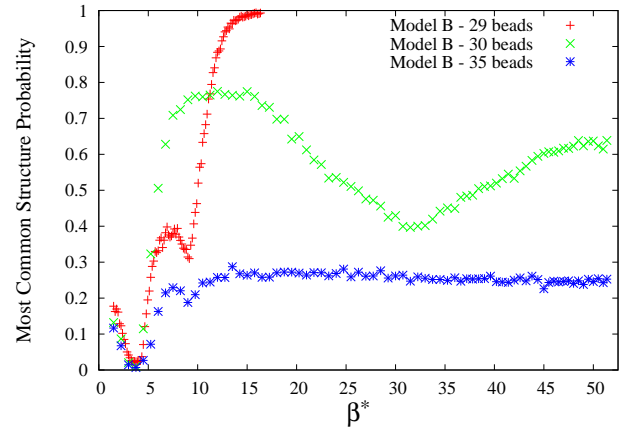


FIG. 9: Variation of the probabilities of the most common structure, f^* , versus the β^* for the chains with 29, 30 and 35 beads. The result of the 29-bead chain from figure 8 is presented here as a reference.

D. Effects of the protein-like chain length

For 25-bead chains, the probability of the most common structure approaches unity at low temperatures, while the longer 35-bead chain did not show this trend. There are two possible reasons for this behavior. First, it is possible that the studied range of temperatures was not sufficiently large to observe the lowest energy configuration for long chains in the simulation. The second possible reason is that the lowest possible energy is not geometrically accessible considering the criteria of model B. The effect of the inaccessibility of the lowest energy configuration is that several structures with the same energy compete for the highest probability. While the configurational entropies of these structures are somewhat different, there is no configuration with a much higher entropy than all the other structures with the same en-

β^*	the most common structure	$f_{\text{obs}}(\%)$
1.5	No Bond	11.7 ± 1.3
5.25	BF BZ Bd Bh FJ FV FZ Fd Fh JN Jd Jh NR Nd RV VZ Zd dh	7.2 ± 0.9
9.0	BF BZ Bd Bh FJ FV FZ Fd Fh JN Jd Jh NR Nd RV VZ Zd dh	18.8 ± 1.5
16.5	BF BR BV BZ Bh FJ FZ Fd Fh JN Jd Jh NR Nh RV Rh VZ Zd dh	25.8 ± 1.8
31.5	BF BR BV BZ Bh FJ FZ Fd Fh JN Jd Jh NR Nh RV Rh VZ Zd dh	24.7 ± 1.6
53.63	BF BR BV BZ Bh FJ FZ Fd Fh JN Jd Jh NR Nh RV Rh VZ Zd dh	23.6 ± 1.6
β^*	the second most common structure	$f_{\text{obs}}(\%)$
1.5	dh	2.3 ± 0.6
5.25	BF BR BV BZ Bd Bh FJ Fd Fh JN Jh NR Nh RV Rh VZ Zd dh	5.3 ± 0.9
9.0	BF BR BV BZ Bh FJ FZ Fd Fh JN Jd Jh NR Nh RV Rh VZ Zd dh	15.4 ± 1.5
16.5	BF BZ Bd Bh FJ FV FZ Fd Fh JN Jd Jh NR Nd Nh RV VZ Zd dh	14.4 ± 1.4
31.5	BF BZ Bd Bh FJ FV FZ Fd Fh JN Jd Jh NR Nd Nh RV VZ Zd dh	16.7 ± 1.4
53.63	BF BZ Bd Bh FJ FV FZ Fd Fh JN Jd Jh NR Nd Nh RV VZ Zd dh	15.2 ± 1.3

TABLE VI: Most common configurations of the model B 35-bead chain.

ergy, and hence none of their maximum structural probabilities approaches unity in the accessible temperature range. It turns out that the second scenario is much more plausible. To understand why, it is helpful to consider the thermodynamic characteristics of model B for other chain lengths. For chains of length 15, 20, 25, 29, 30 and 35, the maximum number of attractive bonds are 3, 5, 8, 12, 17 and 23, respectively. The temperature dependence of the probability of the most common structure for these cases is shown in Figs. 8 and 9.

One sees in Fig. 8 that for chains with 15, 20, 25 and 29 beads, after going through one or two minima, the probability of the most common structure f^* approaches unity at low temperatures. In these cases, the most probable configurations are also the ones with the lowest energy, i.e., with the maximum number of attractive bonds. For the 29-bead chain there is a distinctive peak in the probability of the most common structure at $\beta^* \approx 7.5$, which can be explained by the large entropy difference between the most common structure with 11 bonds and the most common structure with 12 bonds, which allows the 11-bond configuration to become the most common structure for $4.35 \leq \beta^* \leq 9$. Apparently, at $\beta^* = 9$, the energy difference becomes equal to the entropy difference times T^* , so that for $\beta^* > 9$ the structure with 12 bonds becomes the most common structure.

Fig. 9 shows that the situation is quite different for longer chains. For the 30-bead chain, the maximum possible number of bonds is 17, but no such structure was observed in the simulations, even when using different numbers of replicas, different PT temperature sets and different ranges of temperatures. This strongly suggests that it is impossible to satisfy the geometric constraints needed to form all possible bonds. Once the geometric constraints cannot all be satisfied for one particular chain length, this automatically implies that they can also not be satisfied for longer chains. Indeed, in the 35 bead case, the lowest energy configuration is also not observed.

As can be seen in Fig. 9, when $4.5 \leq \beta^* \leq 7.5$, the probability of the most common structure increases for the 30-bead chain (similar to the behavior observed in 15, 20, 25 and 29 beads chain systems). The probability of the most common structure then remains more or less unchanged up to $\beta^* \approx 15$. After this plateau region, the probability decreases until reaching a β^* value at which the probability of the two most common structures becomes equal (in this case, these are the 15-bond structure with the highest entropy and the 16-bond structure with the highest entropy), which can be seen as a minimum in the graph. After passing this local minimum, the structure with 16 bonds becomes the most common structure. However, because there are at least six structures with 16 bonds, the probability of the most common structure is not close to one even at very low temperatures. One explanation is that the structure with 17 bonds is geometrically prohibited, leading to several energetically degenerate configurations with 16 bonds to become common at low temperatures (their relative populations depending on configurational entropy differences).

A second argument for the geometric frustration of the lowest energy configuration for larger chain lengths can be found by slowly relaxing the geometric restrictions imposed by the range of interaction of the attractive bonds in the model. If the configuration is geometrically prohibited, then by slowly increasing the bonding distance one should find a critical value of the range at which the configuration suddenly becomes accessible, and since its energy is lower than any other structure, that configuration should at the same time suddenly become a very common, if not the most common, structure.

The attractive bonds can be formed at a range $4.6\text{\AA} \leq r_{ij} \leq 5.8\text{\AA}$ ($\sigma_1=4.6\text{\AA}$ and $\sigma_2=5.8\text{\AA}$), where r_{ij} is the distance between beads i and j . To change the attractive range, only σ_2 was increased. At $\sigma_2 = 6.2\text{\AA}$, it was possible to observe the lowest energy configuration for the 30 bead chain (with 17 attractive bonds) at low temperatures, while this structure was not observed for the

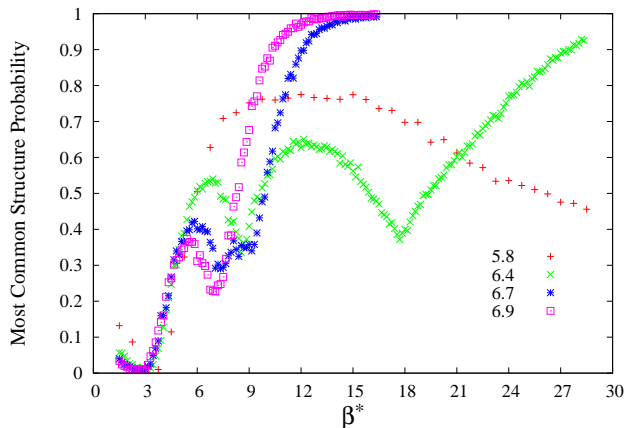


FIG. 10: Variation of the probabilities of the most common structure versus the β^* for the 30-bead chain for different attractive bond interaction distances (increasing σ_2 from the initial 5.8 Å to 6.4 Å 6.7 Å and 6.9 Å

runs with $\sigma_2 \leq 6.1$ Å. Figure. 10 illustrates this by plotting the probability of the most common structure as a function of temperatures for several values of σ_2 . For $\sigma_2 = 6.4$ Å, the probability of the 17 bonds structure approaches one around $\beta^* = 27$, and by increasing the value of σ_2 , this occurs at lower β^* , since the entropic barriers between the low energies configurations, such as the configurations with 15 bonds and 16 bonds, become smaller. The first bump in Fig. 10 represents a temperature region where the structure with 15 bonds becomes the most probable configuration, and the second bump occurs at higher β^* values, where a 16-bond configuration becomes the most probable structure. Since the entropy difference between the configurations with different energies becomes smaller for larger σ_2 , this range of β^* , where the structure with 15 bonds becomes the most common structure, becomes smaller for larger σ_2 values as can be seen for $\sigma_2 = 6.7$ Å and $\sigma_2 = 6.9$ Å in Fig. 10.

We conclude that for chains smaller than 30 beads the landscape consists of one deep funnel at low temperatures that contains several minima. The funnel becomes steeper by decreasing the temperature. At very low temperatures the landscape consists of a smooth funnel with a very deep global minimum representing the configuration with the maximum number of bonds. But for chains longer than 29 beads, the landscape of the longer chains does not consist of one deep funnel, even for low temperatures. Rather, it consists of several minima or channels between which there are entropic barriers that increase with increasing chain length.

IV. CONCLUSIONS

In this work two different models of a protein-like chain that differ primarily in the number of attractive interactions were introduced and the characteristics of their free

energy landscape was analyzed. Fewer bonding interactions are present in the second model (model B), leading to a system with less frustration and a free energy landscape that possesses fewer local minima. The models were designed to encourage the formation of helical secondary structural elements and such helices were observed in model B at low temperatures. For long enough chains (> 17 beads), model B also allows a tertiary structure.

It was shown that for model B, the free energy landscape of the 25-bead chain has a smooth funnel that has important effects on both the dynamics and the thermodynamics of the system. In this model, the free energy landscape at low temperatures contains a deep valley with several minima around it located inside one basin. As the temperature decreases, the deepest point of the funnel becomes deeper, while the minima around the deepest point become shallower. This trend continues until a temperature is reached in which all local minima in the free energy landscape have vanished and only a single global minimum exists. In contrast to Model B, Model A does not exhibit a preference for a specific native structure at low temperatures. This may be attributed to several factors, such as the lack of rigidity of the chain in this model, several large entropic barriers, and the possibility of having many structures with the same energy.

It was shown that the relative configurational entropy is temperature independent. Hence, using the populations of the configurations at different temperatures, the relative free energy and entropy of any pair of configurations can be calculated. From the free energies of different structures at the studied temperatures, the populations of all configurations at any temperature were predicted and verified against simulation results. These results agree reasonably with the simulation results, which shows one of the great advantages of using discontinuous potentials to study the free energy landscape.

In model B, the single funnel morphology of the free energy landscape persists for chains up to 29 beads long. However, for chains of 30 beads or longer, the simulation results strongly suggest that the structure satisfying all possible attractive bonds is geometrically prohibited, while at the same time, the entropic barriers between the configurations with different energies become larger. For long chains, the landscape at low temperatures consists of a few distinct channels that are relatively close to each other but separated by high barriers.

The observed landscape can provide insight into the shape of the landscape of actual proteins. While for small chains the native structure seems to be the lowest free energy structure, the existence of several distinct funnels in the landscape of long chains suggests the possibility that the native structure of real proteins is not necessarily the lowest free energy structure but may correspond to a configurational basin that can be accessed easily during the folding dynamics. Another factor that should be considered for long proteins is the important effect of temperature on the morphology of the landscape. In our

study, the basin containing the global minimum becomes steeper as the temperature decreases for short chains. However, for longer chains, the basin becomes steeper while the deepest point of the landscape can shift from one configuration to another configuration with slightly different bonds over the same temperature range. Thus, for long proteins, the structure may be more sensitive to temperature fluctuations and by slightly changing the temperature the thermodynamically stable configuration can shift to a configuration that differs substantially.

The simulation results presented here can be used to analyze the dynamics of the protein-like chain by computing the first-passage time solution for the transition rates among the individual microstates. The individual rates between microstates can then be incorporated into a Markovian model of the relaxation of the chain and the

dynamics of the folding process examined to probe how features in the energy landscape determine the relaxation profile of the protein-like chain²³.

Acknowledgments

Computations were performed on the GPC supercomputer at the SciNet HPC Consortium, which is funded by the Canada Foundation for Innovation under the auspices of Compute Canada, the Government of Ontario, the Ontario Research Fund Research Excellence and the University of Toronto.

This work was supported by a grant from the Natural Sciences and Engineering Research Council of Canada.

* Electronic address: hbayat@chem.utoronto.ca

† Electronic address: rzon@scinet.utoronto.ca

‡ Electronic address: jmschofi@chem.utoronto.ca

¹ K. A. Dill, S. B. Ozkan, T. R. Weikl, J. D. Chodera, and V. A. Voelz, *Current Opinion in Structural Biology* **17**, 342 (2007).

² P. E. Leopold, M. Montal, and J. N. Onuchic, *Proc. Natl. Acad. Sci. USA* **89**, 8721 (1992).

³ K. A. Dill, *Curr. Opinion Struct. Biol.* **3**, 99 (1993).

⁴ J. D. Bryngelson, J. N. Onuchic, N. D. Socci, and P. G. Wolynes, *Proteins: Struct. Funct. Genet.* **21**, 167 (1995).

⁵ P. G. Wolynes, J. N. Onuchi, and D. Thirumulai, *Science* **267**, 1619 (1995).

⁶ J. N. Onuchic, P. G. Wolynes, Z. Luthey-Schulten, and N. D. Socci, *Proc. Natl. Acad. Sci. USA* **92**, 3626 (1995).

⁷ J. N. Onuchic, N. D. Socci, Z. Luthey-Schulten, and P. G. Wolynes, *Fold Des.* **1**, 441 (1996).

⁸ K. A. Dill and H. S. Chan, *Nature Structural Biology* **4**, 10 (1997).

⁹ N. D. Socci, J. N. Onuchic, and P. G. Wolynes, *Proteins* **32**, 136 (1998).

¹⁰ B. C. Gin, J. P. Garrahan, and P. L. Geissler, *J. Mol. Biol.* **392**, 1303 (2009).

¹¹ T. McLeish, *Biophys. J.* **88**, 172 (2005).

¹² S. Duane, A. D. Kennedy, B. J. Pendleton, and D. Roweth,

Phys. Lett. B **195**, 216 (1987).

¹³ R. H. Swendsen and J.-S. Wang, *Phys. Rev. Lett.* **57**, 2607 (1986).

¹⁴ C. J. Geyer, in *Proceedings of the 23rd Symposium on the Interface: Computing Science and Statistics* (1991), pp. 156.

¹⁵ M. C. Tesi, E. J. J. van Rensburg, E. Orlandini, and S. G. Whittington, *J. Statist. Phys.* **82**, 155 (1996).

¹⁶ D. J. Earl and M. W. Deem, *Phys. Chem. Chem. Phys.*, **7**, 3910 (2005).

¹⁷ M. V. Athawale, G. Goel, T. Ghosh, T. M. Truskett, and S. Garde, *Proc. Natl. Acad. Sci. USA* **104**, 733 (2007).

¹⁸ A. Bellemans, J. Orban, and D. van Belle, *Mol. Phys.* **39**, 781 (1980).

¹⁹ Y. Zhou and M. Karplus, *Proc. Natl. Acad. Sci. USA* **94**, 14429 (1997).

²⁰ D.-W. Li and R. Bruschweiler, *Phys. Rev. Lett.* **102**, 118108 (2009).

²¹ D. C. Rapaport, *The art of molecular dynamics simulation* (Cambridge University Press, Cambridge, 2004), 2nd ed.

²² L. Hernández de la Peña, R. van Zon, J. Schofield, and S. B. Opps, *J. Chem. Phys.* **126**, 074105 (2007).

²³ H. B. Movahed, R. van Zon, and J. Schofield, in preparation (2012).